AIAA JOURNAL
Vol. 43, No. 4, April 2005

Axisymmetric Jet Shear-Layer Excitation by Laser Energy and Electric Arc Discharges

Russell G. Adelgren,* Gregory S. Elliott,† and Jason B. Crawford‡
Rutgers—The State University of New Jersey, Piscataway, New Jersey 08854
Campbell D. Carter§ and Jeffrey M. Donbar¶
U.S. Air Force Research Laboratory, Wright–Patterson Air Force Base, Ohio 45433
and
Dennis F. Grosjean**
Innovative Scientific Solutions, Inc., Dayton, Ohio 45440

Two energy deposition methods (electric arcing and laser-induced optical breakdown) were used to force and control compressible mixing layers of axisymmetric jets. The effects of energy-deposition forcing methods have been experimentally investigated with schlieren imaging, particle image velocimetry, product formation flow visualizations, and high-frequency pressure measurements. Large-scale structures were forced in perfectly expanded jets with nozzle-exit Mach numbers of 1.38, 1.5, and 2.0, utilizing single pulse-laser energy deposition focused at the nozzle exit. Structures were successfully forced over a range of convective Mach numbers from 0.63 to 0.85 using laser pulse energies from 5 to 40 mJ. The large-scale structure forced by laser perturbation in the Mach 1.38 jet was characterized with detailed measurements of the velocity and vorticity fields and the fluctuating pressure history. The measured convective velocity of the forced structure was approximately 25% above isentropic theory, and the structures had a growth rate 2.1 times the undisturbed shear layer. Also, multiple-pulse electric arc discharges were induced locally at the nozzle exit and investigated with schlieren imaging. Electric arc frequencies ranging from 1 to 18 kHz for the Mach 1.38 jet were investigated with Strouhal numbers from 0.32 to 0.56 having the greatest effect.

Nomenclature

a	=	speed of sound
D	=	jet-exit diameter
f	=	frequency
M_c	=	convective Mach number
p	=	pressure
Re_D	=	Reynolds number based on diameter
Sr_D	=	Strouhal number based on diameter
U	=	velocity
U_c	=	convective velocity of large-scale structures
u	=	x component of velocity
v	=	y component of velocity
w	=	z component of velocity
x_c	=	structure travel distance
Δt	=	delay time from excitation laser pulse
ρ	=	density
σ	=	standard deviation
Ω_z	=	z component of vorticity

Subscripts

corrected	=	corrected quantity
i	=	quantity based on isentropic flow
1	=	quantity in jet core (freestream)
2	=	quantity in ambient outside of jet

Presented as Paper 2002-0729 at the AIAA 40th Aerospace Sciences Meeting, Reno, NV, 14–17 January 2002; received 26 February 2004; revision received 20 August 2004; accepted for publication 5 September 2004.

*Ph.D. Student Rutgers University; currently Major, U.S. Air Force Test Pilot School, Edwards Air Force Base, CA 93524-6485. Member AIAA.
†Associate Professor; currently Associate Professor, Aerospace Engineering, University of Illinois at Urbana–Champaign, Urbana, IL 61801. Associate Fellow AIAA.
‡M.S. Student; currently Engineer, Knolls Atomic Power Laboratory, Niskayuna, NY 12309.
§Senior Aerospace Engineer. Associate Fellow AIAA.
¶Senior Aerospace Engineer. Member AIAA.
**Senior Engineer.

Introduction

IN the mid-1800s a medical doctor attending an evening of chamber music observed orderly fluctuations of a coal gas flame associated with a violoncello during a performance of several grand trios of Beethoven noting that "A deaf man might have seen the harmony."[1] This phenomena of the interaction of tones with fluid dynamics was also investigated by Tyndall, who demonstrated that the structure of a variety of air and liquid jets, not just a flame, were sensitive to musical notes.[2] Since these early observations, the nature of turbulence in shear layers created between two streams of different velocity, whether in planar (i.e., two streams separated by a thin splitter plate) or axisymmetric (i.e., circular jets) configurations, has been investigated. Many computational and experimental investigations have focused on the existence and characteristics of large-scale structures (structures that are on the order of the shear-layer thickness and remain coherent as they convect downstream) and methodologies to enhance or suppress mixing between the two streams depending on the application. The goal of the experiments presented in this paper was to investigate and characterize the forcing of large-scale structures in the shear layer of an axisymmetric jet using energy deposition. In particular, the objectives were to 1) show supersonic jets can be forced using energy deposition; 2) compare effects of single- and multipulse depositions; 3) describe the resulting effects, that is, formation of large-scale structures, on the shear layer; and 4) characterize the observed large-scale structure.

Background

Supersonic Shear Layers and Large-Scale Structures

Throughout the 1960s it had been hypothesized that the shear-layer growth rate was altered as the Mach number increased as a

result of density effects. In 1974 Brown and Roshko[3] performed a set of experiments using gases of different densities in order to test that assumption. One of the major findings contained within the paper written by Brown and Roshko[3] was that large coherent structures dominated the mixing layer. In addition Brown and Roshko[3] found that these large-scale structures travel downstream at a nearly constant rate with the size and spacing between them growing as they convect downstream. This increase in size and spacing occurred discontinuously through processes where these structures joined together in full or in part with neighboring structures. Brown and Roshko concluded that turbulent mixing and entrainment were related to the interaction of these coherent structures and the small-scale turbulence, which further breaks up the ingested fluid promoting molecular mixing.

As already mentioned, it has been known that supersonic (compressible) mixing layers have a much slower growth rate compared to their subsonic (incompressible) counterpart. To correlate this decrease in growth rate to compressibility effects, Bogdanoff[4] and Papamoschou and Roshko[5] provided detailed derivations of a convective velocity and corresponding convective Mach number, based on the differences between the velocities from each of the two streams and the defined convective velocity, and the two speeds of sound. Similar to other researchers[6] this convective Mach number will be referred to as the isentropic convective Mach number M_{ci} and isentropic convective velocity U_{ci}, which is equal for the two streams if they have the same specific heat ratio[5]:

$$M_{ci} = M_{c1} = [(U_1 - U_{ci})/a_1] = M_{c2} = [(U_{ci} - U_2)/a_2] \quad (1)$$

where U_{ci} is given by

$$U_{ci} = \frac{a_1 U_2 + a_2 U_1}{a_1 + a_2} \quad (2)$$

Here subscripts 1 and 2 refer, respectively, to the jet core and freestream values and subscript ci refers to the isentropic convective value. Although the aforementioned convective equations were derived for planar shear layers, the same equations have been applied to axisymmetric jets by investigators[6–8] (even though the axisymmetric jet can support axisymmetric and helical instability modes in addition to the Kevin–Helmholtz instability waves associated with the formation of large-scale structures).[9]

Because of differences found between the theoretical and measured convective velocities, Murakami and Papamoschou[8] postulated an empirical correction to these equations, which are better suited for determining the convective velocity of the large-scale structures. For a supersonic jet without a coflow, the empirical equations give the convection rates as

$$U_{c\ \text{corrected}} = U_1 - M_{c1\ \text{corrected}}\, a_1 \quad (3)$$

$$M_{c1\ \text{corrected}} = M_{ci} + \frac{-\mathrm{d}M_c}{\sqrt{1 + (a_1/a_2)^2}} \quad (4)$$

$$\mathrm{d}M_c = 1.25\, \ell_n(M_{ci}) + 1.11 \quad (5)$$

This empirical relationship was also confirmed in a flow-visualization study. Investigators have modified the convective Mach-number relation to take into account recompression shocks, which might be present within the shear layer at high compressibility levels.[10,11]

In addition to quantifying the compressibility effects on the shear-layer growth rate,[5] flow-visualization experiments by Clemens and Mungal in 1992 (Ref. 12) showed that at $M_{ci} \leq 0.5$ the shear layer contained the two-dimensional structures that are characteristic of the incompressible shear layer. In 1993 Elliott et al.[13] found that the pairing processes typical of an incompressible shear layer was still occurring at $M_{ci} = 0.51$, but was not seen at $M_{ci} = 0.86$. Other investigators have shown the convective Mach number also correlates trends in the turbulence profiles and shear-layer characteristics.[14,15]

Forcing Supersonic Jets

Several recent investigations have shifted attention to the problem of controlling the growth rate of supersonic mixing layers and, subsequently, supersonic jets. Applications of these flow control methodologies sometimes have a goal of enhancing the growth rate of large-scale structures (i.e., for mixing fuel and oxidizers in combustion), whereas other applications need to suppress their formation (i.e., increased jet penetration).[16] For example, Slessor et al. experimentally studied the effect of shear-layer inflow perturbations on the mixing and growth rates.[17] Day et al. have analyzed compressible shear-layer flow instabilities where heat was released.[18] Urban et al. have investigated the velocity fields of a planar compressible mixing layer with induced mixing also with a motivation of enhanced combustion.[19] Another relatively recent application is associated with noise from jets, including the noise attributed to large-scale structures in turbulent shear layers.[20–25]

In 1995 Gutmark et al.[26] wrote a complete review of current control and enhancement techniques up to that point in time. Techniques are classified into three categories: techniques increasing the streamwise vorticity, passive excitation, and active excitation. The first group of techniques for shear-layer growth enhancement relies on increasing the axial or streamwise vorticity. This has been demonstrated by utilizing lobed surfaces,[27] trailing-edge devices,[28,29] tabs,[30,31] and swirl.[32] The effects of these devices on the jet and/or mixing layer are varied and often result in increasing losses after the flow is perturbed.

The term passive excitation is used to describe excitation or control methods that rely on geometric changes to the physical arrangement of a system and are generally optimized for one flow condition. These changes in geometry can take the form of a cavity positioned at the exit of a jet nozzle[33] and paddles or other objects placed in the flow path in order to generate a feedback system.[34] In addition investigators have shown that periodically forcing the shear layer utilizing weak waves from bumps placed on the walls of confined shear layers,[35,36] or by running a secondary parallel injection at off-design conditions,[37] can enhance the grow rate of the shear layer. Also researchers are investigating the use of a Hartmann tube (which employ an underexpanded jet impinging on a cavity) to produce a discrete acoustic tone from 2 to 35 kHz to enhance the formation of large-scale structures in the mixing layer.[16,38] By enabling control of the jet-to-cavity separation and cavity depth, the Hartmann tube could become an active excitation device.[39]

Active excitation systems are generally adjustable to accommodate a range of Mach numbers and flow conditions. Some active excitation techniques include pulsed jet deflection,[40] acoustic driving,[41] and mechanical excitation.[42,43] One technique of active excitation, which is particularly relevant to our current methodology, is the glow discharge, which has been utilized by Martens and colleagues.[44,45] They demonstrated the use of glow discharges to enhance the formation of large-scale structures in planar shear layers with convective Mach numbers of 0.5 and 0.64 by exciting either two-dimensional or oblique instability waves at low-to-moderate Reynolds numbers. These studies not only demonstrated the significant effect on the growth rate and spectral content of the shear layer, but also confirmed previous stability analysis showing that as the convective Mach number increases the dominant instability waves become oblique.[35,46,47] Similarly, Fourguette and Winter focused a modulated CO_2 laser beam, for the purpose of inducing photoacoustic forcing, in the freestream to control the large-scale formation and vortex pairing in low-speed subsonic jets (8 m/s).[48] Unlike the passive methods described earlier, the active techniques are effective over a wider range of flow conditions.

In this experimental study, energy deposition is investigated as a method of enhancing and controlling large-scale structures in the shear layer of axisymmetric jets. Two excitation methods were investigated: a sequence of electric arcs and a focused pulse from a Q-switched Nd:YAG laser. Both methods ionize the flow near the nozzle surface and provide single (laser excitation) or multiple (arc) bursts of excitation to the exit of the jet where the shear layer is formed. As discussed next, this energy deposition forces

the formation of large-scale structures, and these structures can be studied using modern diagnostic techniques.

Electric Arc

Historically, the electric discharge in a gaseous medium has been characterized by the pressure of the gas, the potential of the electric field between the electrodes, and the amount of current flowing between these electrodes. The types of gas discharge have been divided into three categories based on the amount of current flow. Currents ranging up to 10^{-6} A are dark or Townsend discharges. Glow discharges range from 10^{-6} to 10^{-1} A, and arc discharges occur for currents approximately over 10^{-1} A (Refs. 49–51).

When an arc discharge occurs between the anode and cathode, plasma formation with increased ion and electron densities takes place in the arc channel within the gas. Various mechanisms, such as thermionic emission from the cathode, ion collisions with the cathode, and radiation-induced emissions at the electrodes and in the gaseous gap between the electrodes, can generate electrons for the current flow between the electrodes. Once electrons are present in the gap, they are accelerated by the electric field across the gap. As the electrons gain energy, they will begin to collide with atoms and molecules of the gas leading to further ionization and more electrons. If there are a sufficient number of collisions, there will be an electron avalanche and rapid ionization of the gas. An electric arc is generated if this avalanche takes place. Electrons and ions gain energy from the electric field across the anode and cathode. Electrons lose energy to collisions with molecules. Pressure and temperature are increased through the acceleration of ions by the electric field. Within the arc channel, the ion temperature can increase up to the order of 10,000 K, and the electron temperature can be on the order of 50,000 K. The transient or steady-state nature of the discharge along with the equilibrium or nonequilibrium properties between the electrodes all depend on the gas composition and pressure, the material (and temperatures) of the anode and cathode, the circuitry driving the electric field between the electrodes, external and internal radiation sources, and the presence of any magnetic fields.

By controlling these same physical principles, the electric arc can be used as an energy-deposition source into compressible gas flows. This energy source can then in turn be used as an active flow control mechanism. Recently, Buck and Li studied the effect of an electric spark disturbance in a Mach 3 flow.[52] Likewise, the electric glow discharge has been used for flow control. A glow discharge was used as an active shear-layer control by Martens et al. in 1994,[53] whereas Roth et al.[54,55] have demonstrated the use of glow discharges for boundary-layer control.

In this experimental study, the electric arc energy deposition provides a means of perturbation to an axisymmetric jet shear layer. By controlling the frequency of the electrical arc perturbation, a method of active flow control is demonstrated. As will be shown, the electric arc perturbation can enhance the mixing within the shear layer of a supersonic jet and induce the formation of large-scale structures.

Laser-Induced Optical Breakdown

In addition to energy addition through an electric arc, energy was added to the flow through a laser-induced breakdown pulse (through the use of a Q-switched Nd:YAG laser); in both cases the energy was deposited into the shear layer. The deposition of energy into a gas medium with a focused laser beam has been studied since the discovery of a laser-induced spark in 1963 (Ref. 56). Subsequent research since then has led to an extensive list of publications, and this research has been detailed and summarized nicely by Raizer,[57,58] Morgan,[59] and Smith.[60] The overall process, described in greater detail by Raizer, starts when a laser beam with sufficient power is focused and a sufficient radiation flux density is achieved, leading to a discharge (somewhat similar to the electric arc discharge). The pressure and temperature of the gas in the region of this discharge will be increased significantly as the energy of the laser is absorbed to cause this so-called laser-induced dielectric breakdown. The energy deposition into a gas by a focused laser beam can be described by four progressive steps: 1) initial release of electrons by a multiphoton effect, 2) ionization of the gas in the focal region by the cascade release of electrons, 3) absorption and reflection of laser energy by the gaseous plasma and rapid expansion of the plasma and detonation wave formation, and 4) the propagation of the detonation wave into the surrounding gas and relaxation of the focal region plasma. Moreover, Adelgren et al.[61] and Dors et al.[62] observed a residual vortex ring produced as a result of the asymmetric plasma formation in quiescent air.

In this study the laser beam is focused on the thoriated-tungsten arc electrode to force the jet shear layer. The electric arc could then be compared to the laser spark experiments by having the same energy-deposition location between the two methods. Root describes the laser-induced breakdown process when a laser beam is focused on a target surface.[63] When the beam is focused on a target surface, the breakdown can initiate at a lower irradiance (W/cm^2) and thus at a lower incident beam energy. The laser irradiation incident on the thoriated-tungsten electrode will generate seed electrons for the transient gaseous plasma generation phase. These seed electrons initiate the breakdown and the plasma formation. Conversely, the initiation of the breakdown in air requires a higher incident energy flux to generate the initial electrons from the gas molecules in air.

Test Apparatus

The experiments were performed at the U.S. Air Force Research Laboratory, Wright–Patterson Air Force Base, Ohio, and in the Rutgers University Gasdynamics and Laser Diagnostics Laboratory. A range of axisymmetric converging and converging/diverging nozzles with exit diameters of 12.7 mm were utilized for various portions of the study. The Mach numbers utilized in the study ranged from 1.38 to 2.0, with the nozzles designed for perfect expansion at atmospheric conditions. Most of the emphasis was placed on the Mach 1.38 jet because the enhancement of mixing in the supersonic case was the primary objective of this experiment and due to limitations of the dry air delivery needed for the higher Mach numbers. Table 1 summarizes the stagnation conditions, exit conditions, Reynolds numbers, and convective Mach numbers and velocities for the jets utilized in this study. A small coflow was provided for seeding purposes for the particle-image-velocimetry (PIV) measurements, as the perfectly expanded jet exhausted into the atmosphere. Crossjet x, streamwise y, and transverse z directions are indicated in Fig. 1. The zero location of the crossjet (x) component is aligned with the edge of the nozzle where the excitation was located.

Initial trade studies varying the location of the laser excitation indicated that it was qualitatively most effective when located as close to the edge of the jet exit as possible. Although initially the laser was focused on the aluminum corner, it was found that this would cause some damage to the aluminum nozzle at the higher energy levels, and therefore the beam from the pulsed Nd:YAG laser was focused onto the tungsten electrode placed at the jet exit. This also made the laser excitation similar in location to the electric arc experiments, which also utilized the tungsten electrode. The Nd:YAG laser could provide only a single pulse but at much higher energies than possible from the arc (given limitations of the power supply). The excitation beam was focused with a 250-mm focal length lens (resulting in a focal diameter of approximately 0.1 mm). The Nd:YAG laser was frequency doubled to a wavelength of 532 nm with a temporal pulse width of about 10 ns and a repetition rate of 10 Hz. At this pulse frequency, each perturbation can be analyzed independently; the pulses are considered as isolated events because the separation distance between pulses in the shear layer is quite large ($\approx$25 m). The amount of energy delivered by the excitation pulse was measured within $\pm$0.5 mJ using an Ophir Optronics 30A-P-SH meter. Timing with the flow diagnostics was controlled with a Quantum Composer pulse generator.

The arc for the jet experiments was produced using a Velonex Model 360 High Voltage Pulse Generator (HVPG) equipped with a V1728 plug-in module, providing a maximum pulse output of 3 A at 10 kV. The HVPG was triggered using an 8013B pulse generator to give an "envelope" of pulses, configured to a burst of 20 pulses, at frequencies from 1 to 18 kHz ($\pm$0.1 kHz), every tenth of a second. The arc was created across a 1-mm gap between the lip of the

Table 1 Test conditions

Quantity	Case 1	Case 2	Case 3
Exit Mach number	1.38	1.50	2.0
Stagnation pressure, MPa	0.31 ± 0.003	0.37 ± 0.003	0.79 ± 0.003
Stagnation temperature, K	295 ± 3	295 ± 3	295 ± 3
Re_D	$6.04 \times 10^5 \pm 0.14 \times 10^5$	$7.02 \times 10^5 \pm 0.15 \times 10^5$	$1.26 \times 10^6 \pm 0.19 \times 10^5$
U_1, m/s	404 ± 4	429 ± 3	513 ± 3
U_{ci}, m/s[a]	218 ± 2	234 ± 2	294 ± 2
M_{ci}^a	0.63 ± 0.01	0.68 ± 0.01	0.85 ± 0.01
$U_{c\ \text{corrected}}$, m/s[b]	339 ± 5	373 ± 4	482 ± 3

[a]Calculated from Eqs. (1) and (2). [b]Calculated from Eqs. (3–5).

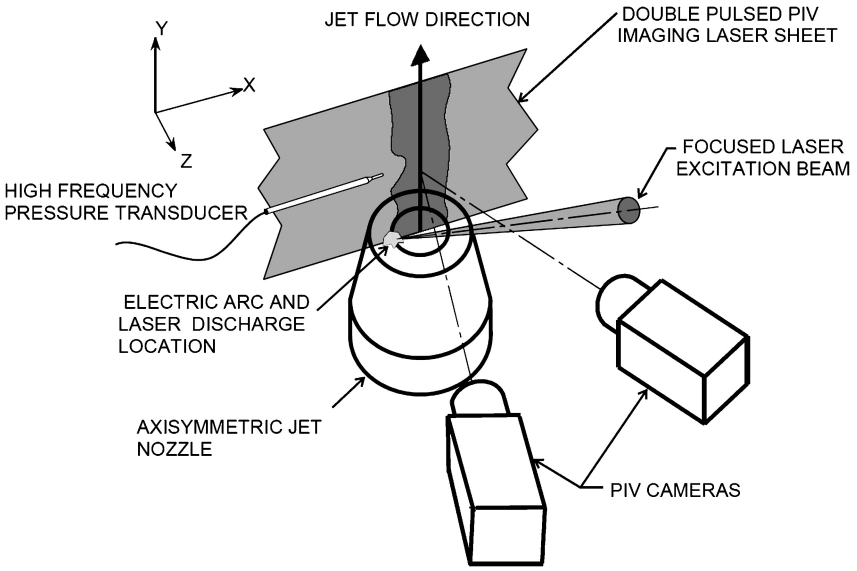

Fig. 1 Test apparatus showing the axisymmetric jet and the PIV instrument for measuring three components of velocity.

nozzle exit and a 1-mm-diam, 2% thoriated-tungsten welding rod. A 3.3-kohm resistor was placed in series with the arc to limit the current and match the impedance of the HVPG. The breakdown of the arc occurred at approximately 4 kV on the leading edge of the pulse; the arc voltage reduces to 50 V once the arc is formed. The voltage drop of the arc is determined by the physics of the plasma created, while the current is primarily a function of the power-supply voltage and series resistor. Energy deposition into the arc was approximately 1 mJ/pulse.

The schlieren images were taken in the standard Z-path arrangement with 150-mm-diam concave mirrors with a focal length of 2 m. The images were recorded on a PixelVision back-illuminated charge-coupled-device (CCD) camera with a resolution of 512×512 pixels. Background and flat-field images were taken to correct for uneven illumination and improve the image quality. A flash lamp provided a light pulse with a temporal pulse width of about 1 μs, effectively freezing the motion of the flow.

A planar Mie-scattering technique was additionally used to image the laser perturbed shear-layer structure. A single pulsed Nd:YAG laser beam (wavelength of 532 nm) was formed into a sheet at the same location as the double-pulsed laser sheet used for the PIV measurements (discussed in the following section). A Princeton Instruments intensified CCD camera was placed normal to the laser sheet to record the images of the Mie scattering from condensation "particles" produced in the jet shear layer. The jet was exhausted into the moist ambient air, whereby condensation formed in the shear layer as a result of entrainment of the moist air into the cooler jet. This method of flow visualization has been utilized previously in the study of supersonic mixing layers and is termed product formation by Clemens and Mungal who first utilized the technique.[12]

A LaVision three-component PIV system was used to measure the complete velocity field at each measurement plane. This system uses two views (i.e., cameras) in a stereoscopic format to construct all three velocity components (Fig. 1). Through the imaging of a target placed at the probe region, the LaVision software corrects the images for oblique optical distortion and aligns the two fields of view. From the two frames and with knowledge of the delay time of the two laser pulses, the velocity field is calculated using cross-correlation techniques. The spatial resolution of the cameras is 1280×1024 pixels, and the images were digitized to 12-bit resolution. The two illumination pulses were from a pair of Q-switched Nd:YAG lasers, each providing about 120 mJ/pulse. Cylindrical and spherical optics were used to form a 1-mm-thick laser sheet, which was passed transversely through the jet so that the compressible shear layer could be visualized. Both the supersonic jet and coflow were seeded with 0.5-μm aluminum-oxide particles; based on this size, the particles sufficiently followed the flow structures. The uncertainty in the average velocity measurements presented here is estimated to be better than $\pm 2\%$ for the PIV system, field-of-view characterization, and processing algorithms used in this study.

Additionally, pressure measurements were recorded outside of the jet shear layer with an Endevco pressure transducer mounted on a probe, as illustrated in Fig. 1. Power was supplied to the transducer with an Endevco Model 106 power supply, and an Endevco Model 109 signal conditioner amplified the transducer signal. The signal was filtered with a Krohn-Hite 3103A filter with cutoff high and low frequencies of 70 kHz and 10 Hz, respectively. The output from the signal conditioner was displayed on a 500-MHz oscilloscope, and the data were digitally recorded through a National Instruments GPIB-PCMI card connected to a laptop PC. The pressure transducer was statically calibrated over the range of expected pressures.

Results and Discussion

Laser Excitation

One goal of this study was to investigate the ability of the focused laser to excite the jet. To determine the effectiveness of laser excitation over a range of Mach numbers, a single laser excitation pulse was focused on three different jets. Figures 2 and 3 show a typical instantaneous image with no laser excitation (panels a) and average streamwise images without (panels b) and with (panels c–e) 16.6 mJ of laser excitation for the Mach 1.38 (Fig. 2) and Mach 2.0 (Fig. 3) jets. The flow is from left to right with only the side of the shear layer visualized, which will experience laser excitation in the later images (i.e., the high-speed core of the jet is located at the top of the image). The streamwise axis y is nondimensionalized by the jet diameter D. In considering typical instantaneous images for the two Mach numbers (Figs. 2a and 3a), the lower Mach number shows clear evidence of large-scale structures. Although the shear layer is not planar, but axisymmetric, the structures have characteristics similar to those reported by Brown and Roshko in 1974, with definable core and braid regions. Also as reported by other investigators of planar shear layers,[5,10,12–14] one would expect that as the convective Mach number increases the large-scale structures become less organized; therefore, for the jet with the lower convective Mach number ($M = 1.38$) the structures appear more organized than at the higher convective Mach number (i.e., at $M = 2.0$). In a similar Mach-number range, this trend has been reported and quantified (using two-dimensional cross-correlation definitions) by Thurow et al.[6] Because neither the large-scale structures observed at the lower Mach number or the less organized structures at the higher convective Mach number are spatially stable, as the instantaneous images are averaged (Figs. 2b and 3b) the shear layer shows a continuous growth of the mixed region as marked by the product formation particles. Again the shear layer of the axisymmetric jet has similar characteristics to planar shear layers with the growth rates of the jet with a lower Mach number (and consequently convective Mach number) greater than the jet with a higher Mach number.

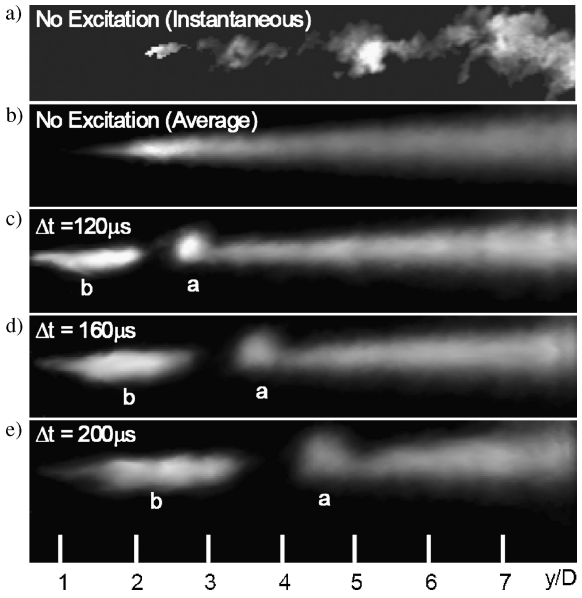

Fig. 2 Streamwise images of a compressible shear layer from a Mach 1.38 axisymmetric jet ($M_C = 0.63$): a) instantaneous, b) average, and c–e) phase-averaged. Time delays for the phase-averaged images are between the laser excitation and image pulses.

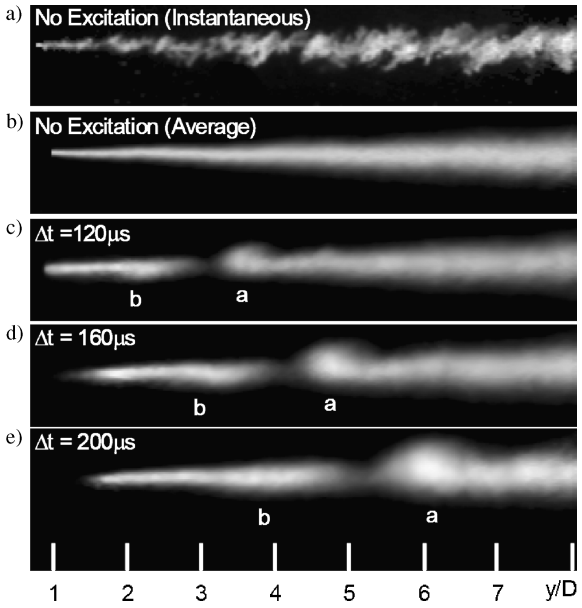

Fig. 3 Streamwise images of a compressible shear layer from a Mach 2.0 axisymmetric jet ($M_C = 0.85$): a) instantaneous, b) average, and c–e) phase-averaged. Time delays for the phase-averaged images are between the laser excitation and image pulses.

One-hundred-fifty instantaneous images were collected of the forced shear layer at each time delay and phase averaged. The time delay between the excitation pulse and imaging pulse was varied from 120 to 200 μs in increments of 10 μs for the Mach 1.38 and Mach 2.0 nozzles, although only images at 40-μs increments are shown here. All of the images with excitation show a large-scale coherent structure in a stable position in the compressible shear layer. This forced large-scale structure has been labeled "a" in the figures. The structure grows as it travels downstream. For a given time delay from the laser excitation pulse, a phase-averaged structure is present at a stable position, indicating that it is a result of the excitation pulse. Recall that in the unexcited shear layer the structures are "smeared" out by the averaging process. Therefore the existence of the large-scale structure in the phase-averaged images is an excellent indication of the ability of the laser excitation to create and control the large-scale structure. Furthermore, this structure has a distinct vortex core and braid region followed by an elongated secondary structure (labeled with "b" in each image), which extends further into the ambient air. This large-scale structure is created even for the higher convective Mach number, which showed little indication of a large-scale structure without excitation, but appears to be more elongated and evident at the lower Mach number. In general the lateral x length scale of the core vortex structure is approximately 40% greater than the unexcited shear-layer thickness at the same streamwise location. Previously it was shown that multiple laser pulses appropriately timed can induce interactions such as pairing between successive structures.[64]

Another quantity of interest is the convective distance traveled by the large-scale structure's core, which is plotted in Fig. 4 against the time delay between the excitation and imaging pulses for the

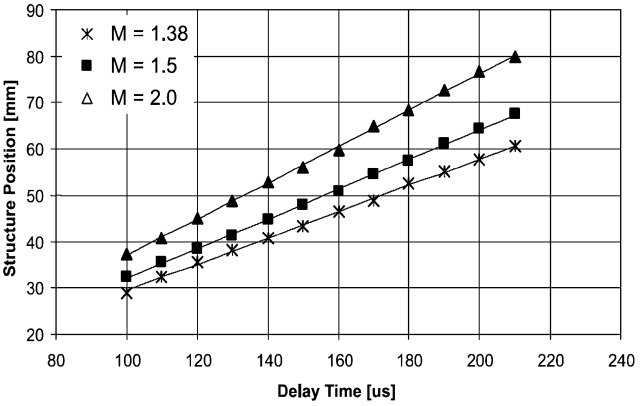

Fig. 4 Large-scale structure position measured from flow visualizations at varying times and Mach numbers.

three Mach numbers studied. The distances traveled by the core region were calculated (within ±0.4 mm) based on the centroid of the core. With knowledge of the time delay between the excitation pulse and the delayed imaging pulse (Δt) and the distance the structure travels x_c, the measured convection velocity can be calculated by

$$U_{c(\text{measured})} = x_c/\Delta t \tag{6}$$

The isentropic and corrected convective velocities for all three Mach numbers are given in Table 1 with the measured values along with those from other studies (at approximately the same Mach number) given in Table 2. It can be seen from Table 2 that the measured convective velocity from our study is approximately the same as that of other studies (within 10%). Compared with the theoretical isentropic U_{ci} and corrected $U_{c\text{-corrected}}$ convective velocities from Table 1, however, the measured values are higher and lower by an average of approximately 25 and 16%, respectively.

Table 2 Convective velocities measured from flow visualizations

Source	Mach 1.38	Mach 1.5	Mach 2.0
Present study, m/s	284 ± 4	321 ± 8	393 ± 12
Ref. 6, m/s	266 ($M = 1.28$)	——	402, 190
Ref. 7, m/s	——	352	——

Now that it has been shown qualitatively that laser energy deposition can be utilized to force large-scale structures in a compressible mixing layer, the velocity content of the structure will be investigated. Measurements have been taken using the aforementioned stereoscopic PIV system. Figure 5 shows the three Cartesian contour plots of the components of velocity with the u–v vector field overlaid (with the convective velocity subtracted from the v component in the vector plots) and the z component of vorticity for the unperturbed Mach 1.38 jet. The jet is perfectly expanded and is free of shocks. (This was also confirmed previously by schlieren images for the unperturbed jet.) The jet flow shown in the PIV plots is oriented from bottom to top, and the positive z axis points out of the page (see also Fig. 1). The PIV data range from 2.5 to 7 diameters downstream of the nozzle of the jet, which is where the large-scale structure will be for the investigated time delays. The z component of vorticity is computed from the averaged velocity fields. The averages are computed from an ensemble of 500 instantaneous PIV data sets. The jet core velocity is measured to be 400 ± 8 m/s at the bottom of the image, which is within 1% of the isentropic value of 404 m/s. The x and z components of velocity are less than 3% of the core. These small velocity components could be caused by a slight tilt in the PIV sheet, insufficient sample size, or other PIV

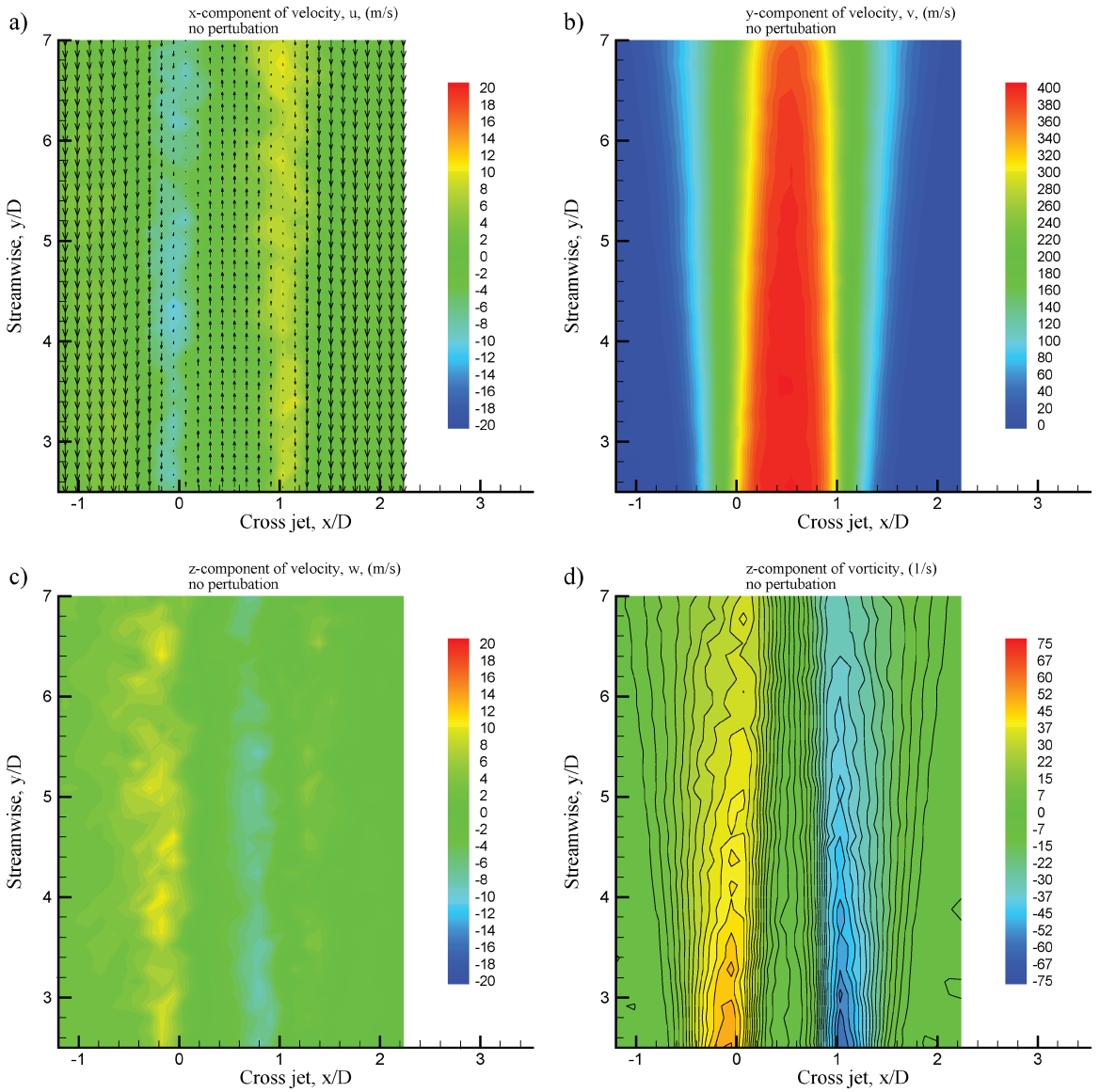

Fig. 5 Contour plots of three Cartesian velocity components [a) u, b) v, c) w, with u–v vector field overlaid on the u component with the convective velocity subtracted] and d) z component of vorticity for the Mach 1.38 jet with no perturbation.

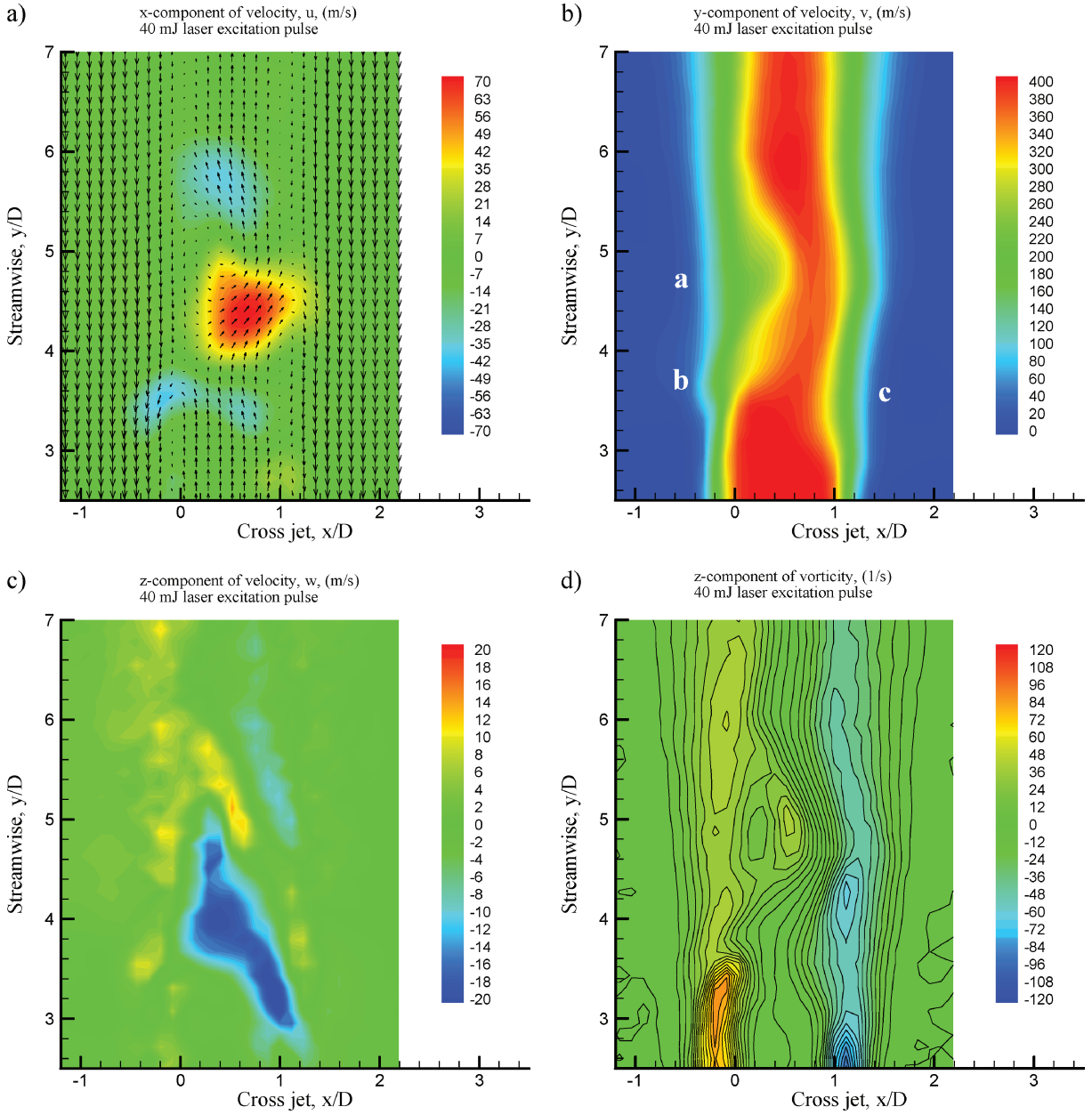

Fig. 6 Contour plots of three Cartesian velocity component [a) u, b) v, c) w, with u–v vector field overlaid on the u component with the convective velocity subtracted] and d) z component of vorticity for Mach 1.38 jet 220 μs after a 40-mJ laser spark perturbation.

inaccuracies. The vorticity is at its maximum in the shear layer at the most upstream position. As the shear layer grows in thickness, the peak of the vorticity decreases 39%, primarily because now the same streamwise velocity difference is spread over a larger shear-layer thickness. Furthermore, the linearity of the contours in the y direction of the z component of the vorticity Ω_z shows a linear growth of the mixing layer in the streamwise direction.

Figure 6 gives the u, v, and w velocity components and the Ω_z vorticity component for the Mach 1.38 jet perturbed with a single laser pulse of 40 mJ. Similarly, the u–v vector field has been plotted on top of the u-component contour plots where the convective velocity has been subtracted from the v component in the vector field plots. The velocity components again are an ensemble average of 500 phase-locked instantaneous velocity fields at 220 μs after the laser perturbation. The same probe region is used both with and without perturbation (and for both arcing and laser sparking, i.e., $y/D = 2.5$–8). The y component of velocity (Fig. 6b) v shows the large-scale structure (labeled "a") extending into the jet core. Because of this protrusion of the large-scale structure, the velocity in the core of the jet decreases by 10%. A large effect of the laser perturbation can also be observed in the x component of velocity and the convective vector field, which accentuates the location of the large-scale structures. The opposing directions of the u velocity component indicate a roller-type structure at approximately $y/D = 4.9$, turning the jet core around the structure. The z component of velocity shows an interesting feature as well, although it is fairly weak when compared to the magnitude of the y component of velocity. There appears to be a three-dimensional swirl where the flow is coming out of the plane behind the structure and into the plane in front of the structure. The vorticity component Ω_z shows the field to be thicker in the region of the large-scale structure and with a lower magnitude over the entire structure, as a result of the increase in shear-layer thickness; however, the peak vorticity is approximately the same on the high-speed side of the structure as in the unperturbed shear layer (at the same streamwise location). Also apparent is the head of the secondary structure (labeled "b"), which lags behind the primary core of the large-scale structure as observed particularly in the y component of velocity. The large-scale structure

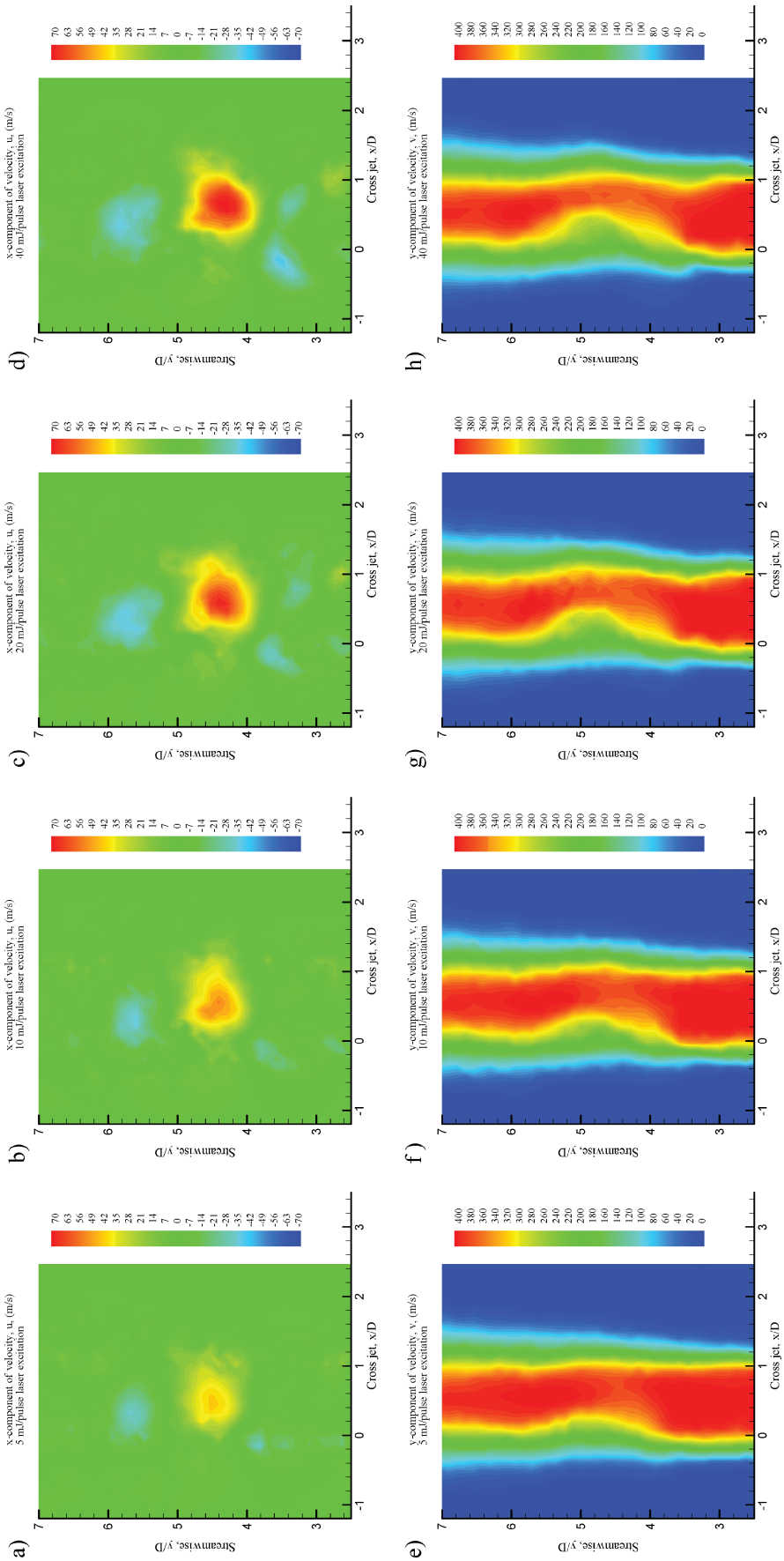

Fig. 7 Comparison of the a–d) *u* and e–h) *v* velocity components for laser perturbations of a, e) 5-mJ/pulse, b, f) 10-mJ/pulse, c, g) 20-mJ/pulse, and d, h) 40-mJ/pulse at 220 μs.

has grown enough that a third (or tertiary) weaker structure (labeled "c") is induced in the shear layer on the opposite side behind the core of the induced structure at $y/D = 3.8$. The vorticity plot also shows the secondary and tertiary structures on the opposing shear layer locally increasing the magnitude of the z-vorticity component by 36% from the baseline value in the shear layer.

Figure 7 compares the average y component of velocity for increasing values of laser pulse energy from 5 to 40 mJ. First, all energy levels show some degree of forcing, creating a stable large-scale structure in the phase-averaged PIV images for the v component of the velocity as the structure extends into the jet core. Defining the size of the structure δ_u by the cross-jet distance x between points at 20 and 80% of the freestream velocity (at the peak of the disturbance), the structure vs the energy of the excitation laser pulse can be plotted (Fig. 8). As observed, the size of the large-scale structure increases with deposition pulse energy level by approximately 43% when the energy is increased from 5 to 40 mJ, but the trend of increasing disturbance size vs energy seems to level off after 20 mJ. The increase in the size and strength of the large-scale structure is also observed in the magnitude change of the positive u component of the velocity induced by structure, as shown in Figs. 7a–7d, which increases with the energy by 65% from 5 to 40 mJ; again, this increase in velocity levels off after 20 mJ. This trend in large-scale structure size is also observed by defining the structure size by its effect on the z component of vorticity (not shown here). Additionally, the secondary and tertiary structures in the opposing shear layer are not as evident at the lower energy levels.

To examine the full spatial extent of the large-scale structure induced by the laser excitation, three-component PIV data were obtained for the 40-mJ/pulse laser excitation across the full volume of the Mach 1.38 jet; this was done only at the time delay of 220 μs (after the excitation pulse). The volume of velocity data was created by 21 planar fields of PIV data taken across the jet in 1-mm increments. The planar fields were phase averaged (50 for each plane location) and then assembled to produce the volume of phase-averaged velocity data in the z direction. Figure 9a shows the deformation to the jet core caused by the laser excitation pulse using the 320-m/s v-component isosurface. The large-scale structure is centered at $y/D = 4.9$. The same axis system is used as for the aforementioned cases. The effect on the core is clearly evident showing

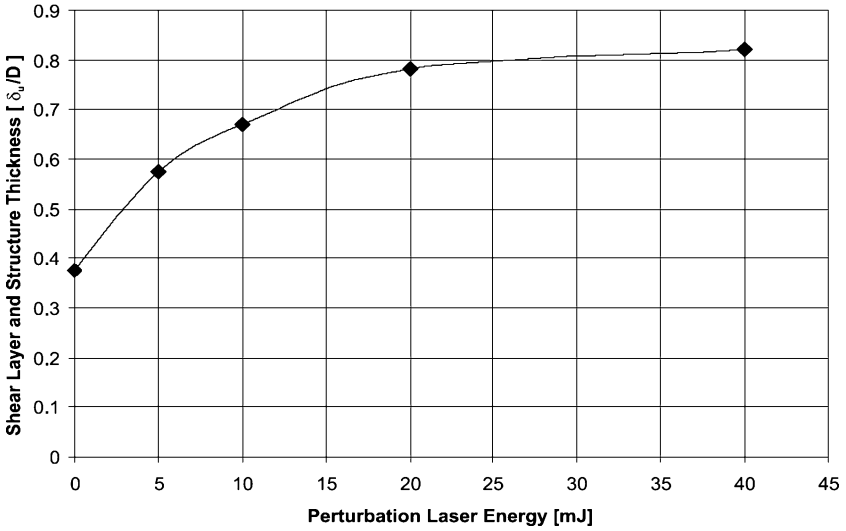

Fig. 8 Shear layer and structure core thickness as a function of perturbation laser energy for a Mach 1.38 jet at 220 μs.

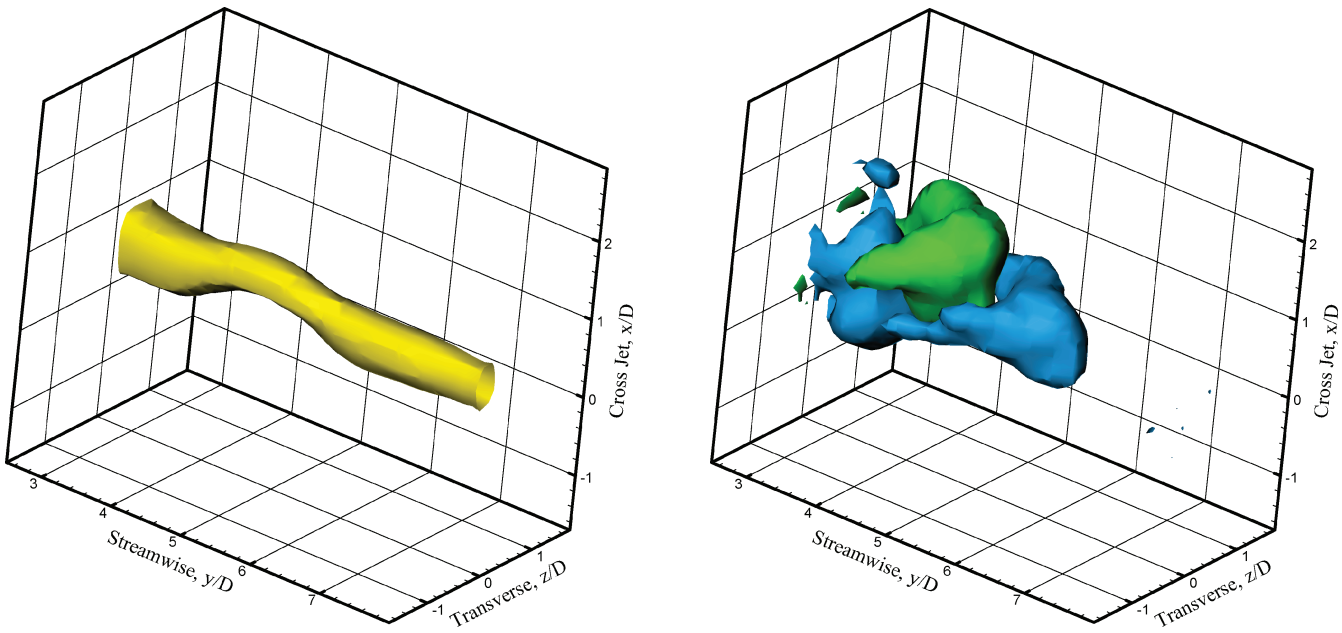

a) v-Component isosufaces **b) u-Component isosurfaces**

Fig. 9 Isosurfaces for v [a) 320 m/s] and u [b) 10 m/s blue and 10 m/s green] components of the velocity for the Mach 1.38 jet 220 μs after a 40-mJ laser spark perturbation.

that it pinches off at the top of the forced structure. The structure extends into the jet core, and the flow in the core moves around the large-scale structure as shown by the isosurface, affecting the opposite side of the shear layer. From the planar results shown earlier, it was found that one of the best ways to view the laser-induced, large-scale structure is to consider the cross-jet x component of the velocity. Figure 9b shows the isosurfaces of the cross-jet x velocity for $+10$ and -10 m/s, shown as green and blue isosurfaces, respectively. These isosurfaces clearly indicate the core of the large-scale structure as defined by the cross-jet x velocities, which point downward in the front of the structure and upward at the back of the structure. The cross-jet x velocity isosurface then wraps around the sides of the structure as the structure is confined by the axisymmetric jet.

Figures 10 and 11 show the time evolution of the jet with the 40-mJ perturbation. In each figure the column corresponds to an instant in time. In each column the first two graphs shown are the u- and v-velocity component contour plots, with the u–v vector field plots (with the convective rate subtracted from the v component) overlaid on the u-component contours. The third graph is the z component of vorticity computed from the velocity data. In this case the velocity data are an average of 50 PIV phase-locked images at each time step, with data taken at every 4 μs (all of which is not shown here). The field of view covers $y/D = 1.4$–6.8. The evolution of the large-scale structure created by the laser energy deposition can clearly be observed as it moves within the mixing layer (Figs. 10 and 11). At $\Delta t = 100$ μs (Figs. 10a–10c) the initiation of the core of the large-scale structure is observed as a kink in the shear layer, which can be seen in y component of the velocity (Fig. 10b) and the z component of vorticity (Fig. 10c). The x component of the velocity (Figs. 10a, 10d, 10g) again shows the strong effect as the jet core goes around the structure. By $\Delta t = 140$ μs (Figs. 10g–10i) the large structure has clearly developed and maintains a similar shape in all properties as

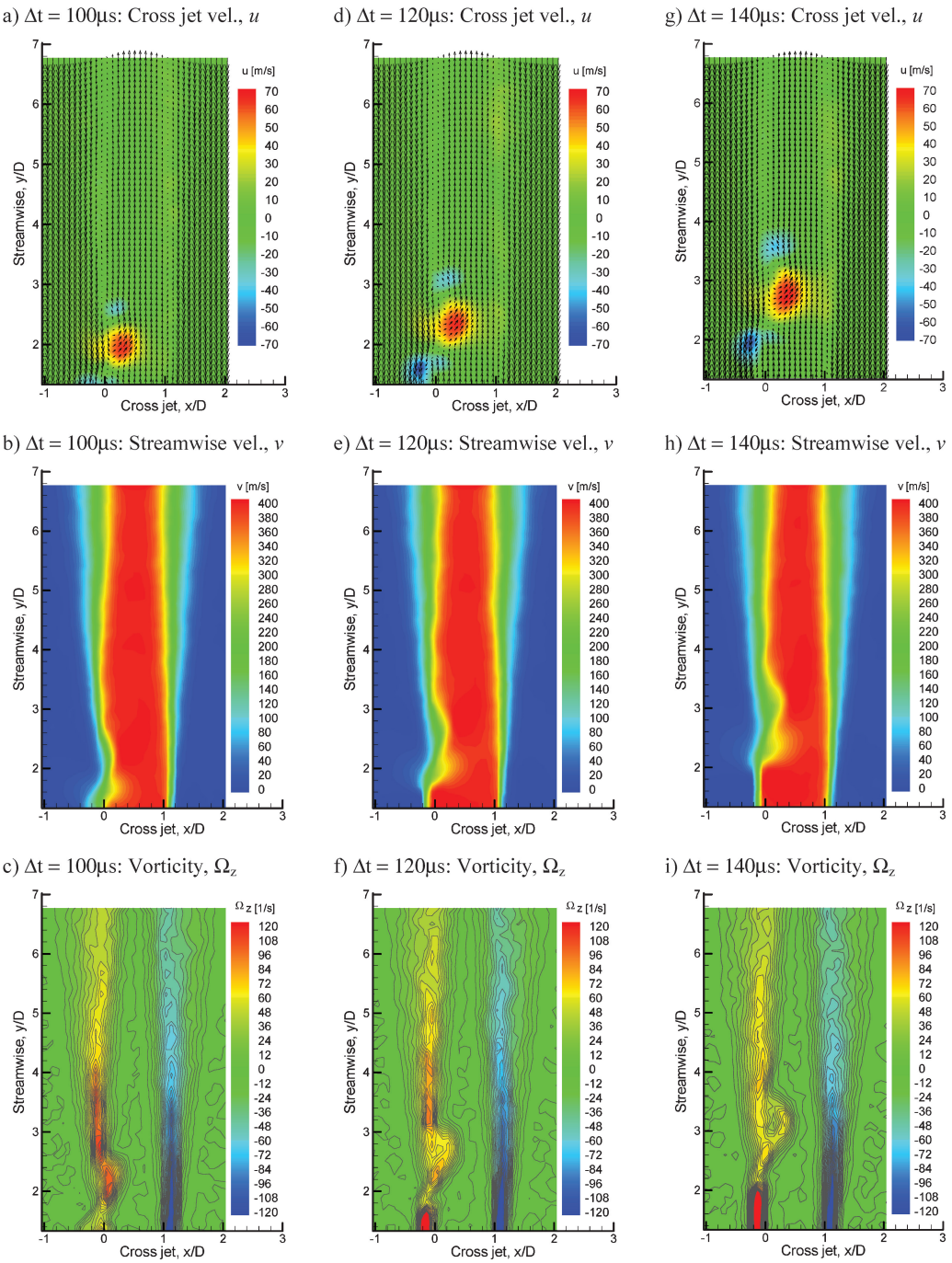

Fig. 10 Temporal evolution of the x component of velocity, u with u–v vectors (a, d, g), the y component of velocity, v (b, e, h), and the z component of vorticity Ω_z (c, f, i), at delay times from the excitation laser pulse of 100 μs (a, b, c), 120 μs (d, e, f), and 140 μs (g, h, i).

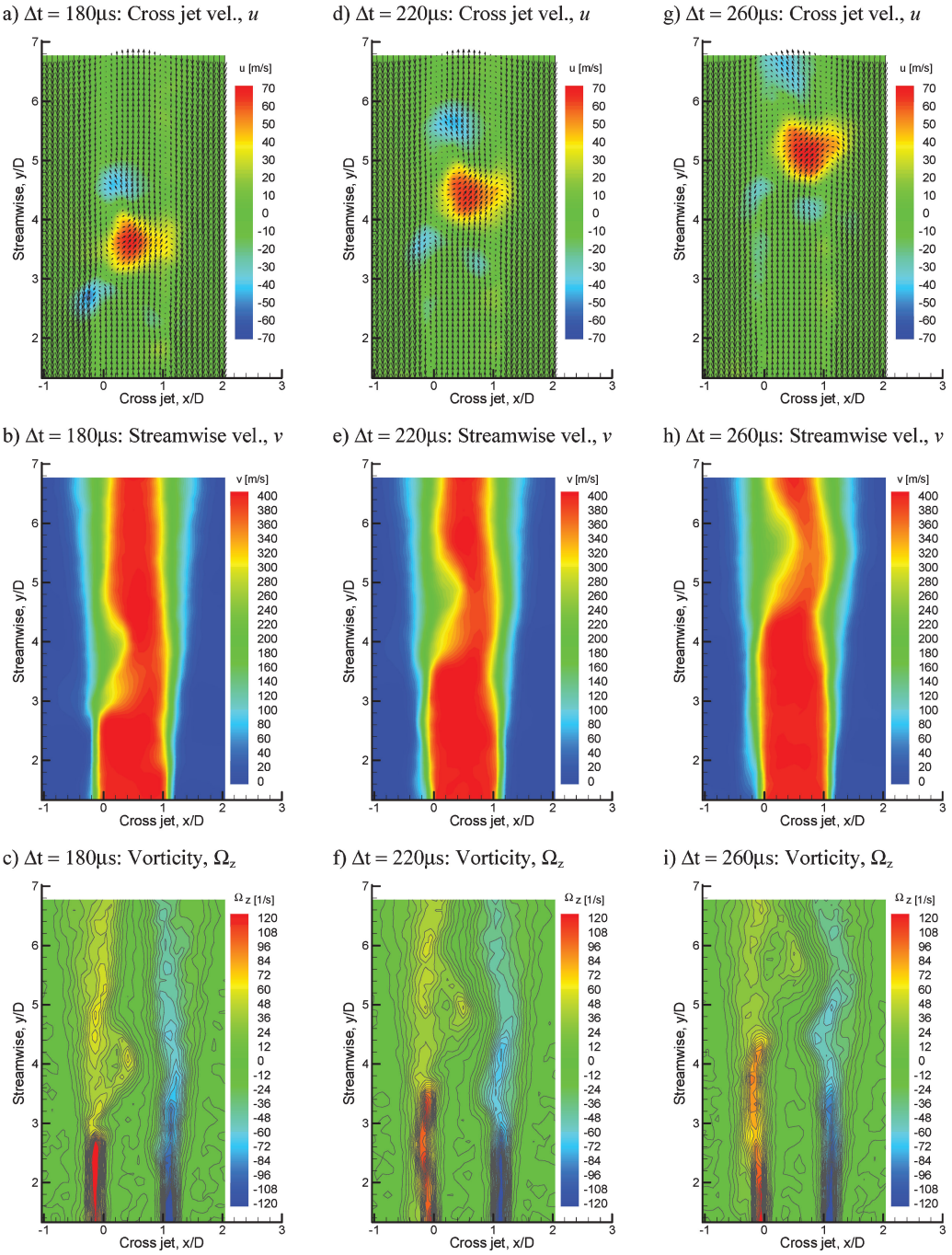

Fig. 11 Temporal evolution of the x component of velocity, u with u–v vectors (a, d, g), the y component of velocity, v (b, e, h), and the z component of vorticity Ω_z (c, f, i) at delay times from the excitation laser pulse of 180 μs (a, b, c), 220 μs (d, e, f), and 260 μs (g, h, i).

it grows and convects downstream. Also, it is quite striking that the magnitude of the x component of velocity on the upstream side of the structure, as the jet is being turned and compressed around the structure, is larger than on the downstream side of the structure, as the flow is expanded and turned back. The effects on the velocity and vorticity of the secondary and tertiary structures do not begin to become evident until later delay times (i.e., 220- and 260-μs results shown in Fig. 11).

To deduce the convective velocity and compare the growth rate of the large-scale structure with the unexcited shear layer, the structure thickness (defined earlier as the distance between the 20 and 80% of the freestream velocity) is plotted with the shear-layer thickness (with an uncertainty of $\pm$0.2 mm) as a function of the streamwise position for each delay time (Fig. 12). As observed here, both the structure and shear-layer growth are linear in this region of the jet. Also, it is quite obvious that the excited structure has a much higher growth rate than the unexcited shear layer. Plotting the ratio of the structure thickness to the unperturbed shear-layer thickness for each streamwise location, it can be observed that the growth rate of the forced structure is approximately constant and 2.1 times larger. The convective velocity can be found by the slope of the line of the structure distance vs time (not shown here). For the PIV experiments, the convective velocity of the structure is found to be 275 m/s $\pm$10%, which is close to that determined from the condensation images, but again above the theoretical value of 218 m/s.

A high-frequency static-pressure probe, oriented as shown in Fig. 1, was utilized to record the pressure trace as the large-scale structure convected across it. The phase-averaged static-pressure plots from the three streamwise locations ($y/D = 2.8$, 4.1, and 5.1) are shown in Fig. 13 for the 40-mJ laser excitation case. Traces

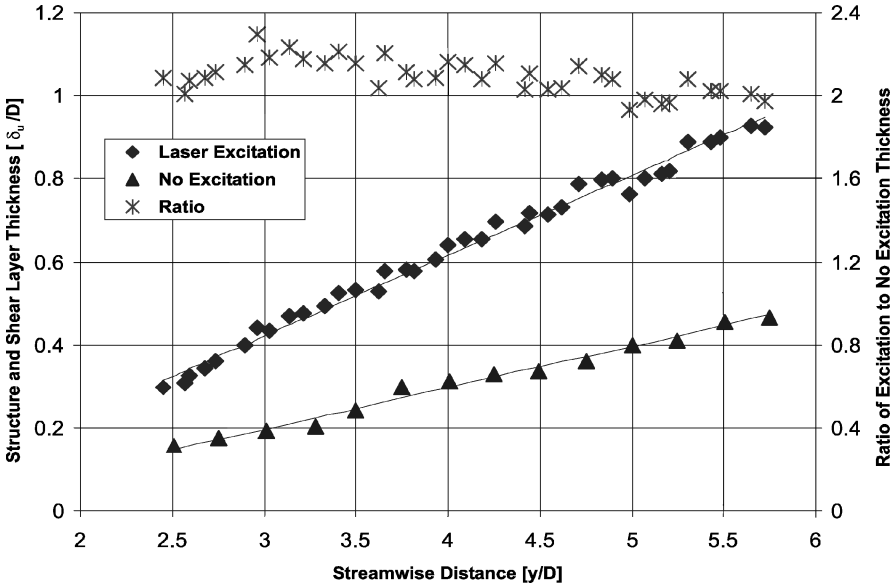

Fig. 12 Shear layer and structure core thickness and the thickness ratio variation with streamwise distance.

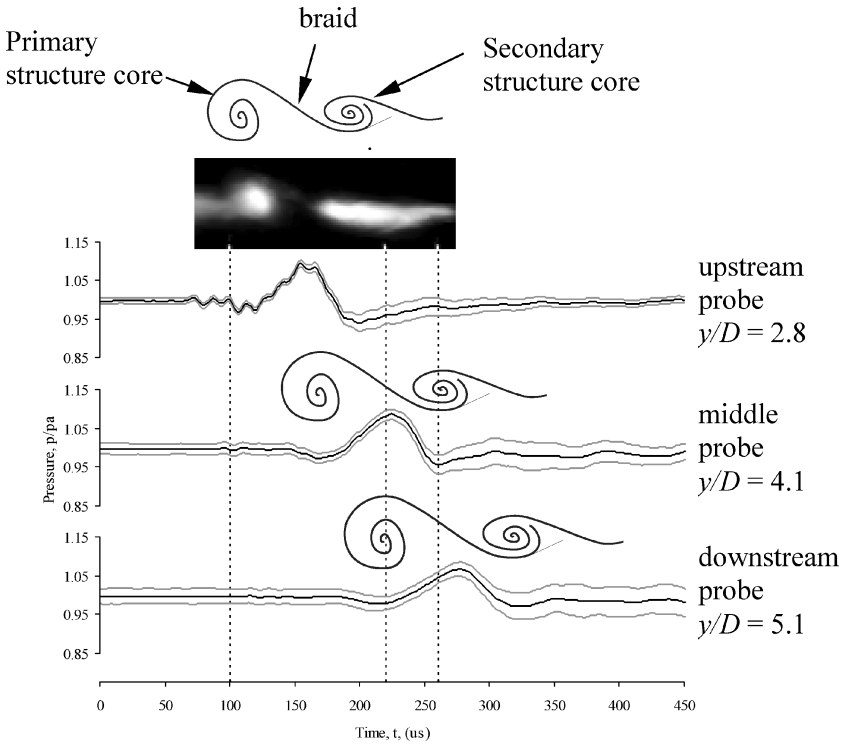

Fig. 13 Static-pressure probe (upstream, middle, and downstream) traces of large-scale structures relative to the time after laser excitation. The three lines for each location show the average value and the average value plus and minus one standard deviation.

indicating the average $\pm 1\sigma$ for the pressure data are also shown on the plots. For reference, the times of 100, 220, and 260 μs are shown on the plots, as well as a flow-visualization image—aligned with the pressure trace by considering the probe position and converting the spatial scale of the image to a temporal scale by dividing by the convective velocity—and a schematic of the primary and secondary structures. All three streamwise locations show a minimum when the cores of the primary and secondary structures pass the probe. A peak pressure is observed when the braid region between the two structures passes, which decreases in magnitude as the structure convects downstream. Considering the model of the large-scale structure as presented by Papamoschou and Roshko[5] and Papamoschou,[65] a peak in pressure in the braid region corresponds to the stagnation point created as the two streams across the shear layer meet in a frame of reference translating with the structure. The minima in the pressure traces correspond to the core regions of the large-scale structures. The average convective velocity of the stagnation point (based on the peak-to-peak pressure data) is 255 ± 6 m/s. This lower convective velocity (vs $\sim$275 m/s) is most probably because the peak pressure occurs closer to the lower-velocity side of the shear layer and therefore travels at a slightly lower velocity.

Electric Arc Excitation

The first task in investigating the arc excitation was to investigate which arc pulse frequencies amplified the growth of the mixing

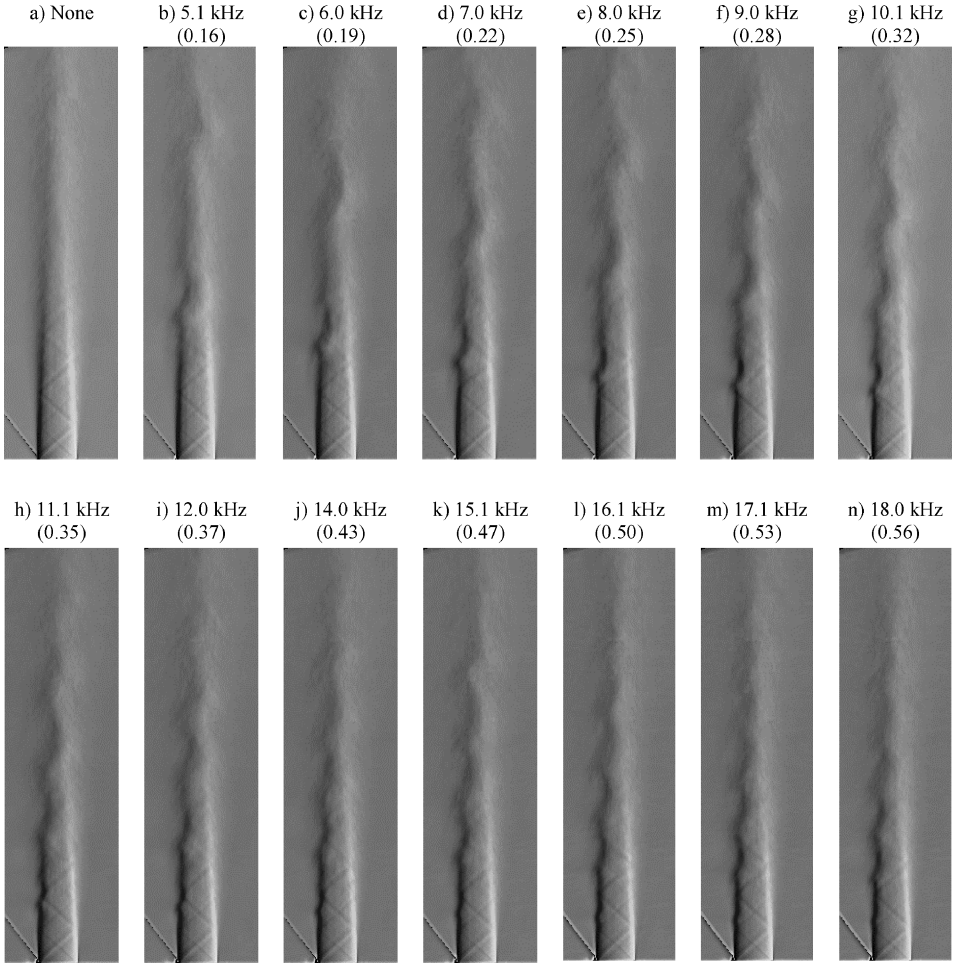

Fig. 14 Schlieren images of electric arc shear-layer perturbation in a mach 1.38 jet a) without excitation and b to n) at varying excitation frequencies from 5.1 to 18.0 kHz. (Top numbers represent the pulse frequency in kilohertz, and bottom numbers in parentheses represent the Strouhal numbers for each case.)

layer. The growth of the mixing layer was qualitatively assessed based on the schlieren images taken for varying arc pulse frequencies. The schlieren images were taken over a range of arc excitation frequencies for each nozzle. Schlieren images with the electric arc perturbation are given in Fig. 14 for the Mach 1.38 nozzle. Each image is an average of 50 frames synchronized to the excitation pulse. The excitation arc pulse is located in the left shear layer just above the nozzle surface. Each schlieren image is oriented with the test nozzle at the bottom of the image and the jet flow direction going from bottom to top. The knife edge for the schlieren system is vertical so the intensity gradient is observed across the shear layer of the jet. The tungsten rod (electrode), described in the Test Apparatus section, can be seen at the lower left of each image. The undisturbed jet is shown at the upper left. Images are shown with increasing arc pulse frequency from top left to bottom right. The spacing in the perturbation to the shear layer decreases as the arc frequency increases, as the figures clearly show. The nondimensional quantity characterizing the forcing frequency to the shear layer is given by the Strouhal number and is expressed by

$$Sr_D = fD/U \tag{7}$$

where D is the characteristic length (the diameter of the nozzle in this case) and U is a characteristic speed of the fluid (here it is the magnitude of the exit velocity of the jet).

For shear layers of subsonic jets, a Strouhal number between 0.25 and 0.5 has been reported as the most amplified forcing frequency.[66] For the Mach 1.38 jet shown in Fig. 14, all frequencies show some perturbation to the shear layer. The first structure in the pulse train can be seen in each of the schlieren images (for all frequencies used). For the lower frequencies, the induced structures in the shear layer are isolated until they grow and begin to interact downstream giving a wavy appearance to the shear layer, similar to what was observed in the glow discharge experiments of Martens et al. for planar mixing layers.[44,45] For the Mach 1.38 jet the most effective, long lasting, and uniform perturbation seems to occur between 10 and 18 kHz, corresponding to Strouhal numbers of 0.32–0.56. Compared to the subsonic jet studied previously with the same arc excitation,[67] the large-scale structures in the Mach 1.38 jet shear layer do not grow as rapidly as indicated by the longer streamwise extent of the jet core for the Mach 1.38 jet. To induce large-scale structures on the same scale as those forced by the laser excitation, a larger energy pulse is presumably needed.

Figure 15 gives the contour plots of the phase-averaged x, y, and z components of velocity with u–v vector field overlaid and the z component of vorticity for the case where the shear layer of the Mach 1.38 jet is excited with the electric arc at 10 kHz. The y component in the vector fields, as in Fig. 15, has the convective rate subtracted. The same coordinate system as described earlier applies (Fig. 1), and the same region of the jet is interrogated with the PIV system. The impact of the arc forcing is most visible on the x component of velocity. The opposing directions of u on either side of the structure indicate a roller structure in the region of $y/D = 4$ and 6. The y component shows only a slight perturbation at $y/D = 4.6$, where the core velocity in this region decreases by 5%. Little or no effect is seen in the z component of velocity w. The confinement of the vorticity component Ω_z appears to have spread, and its magnitude within the shear layer has decreased slightly. Thus, one might say

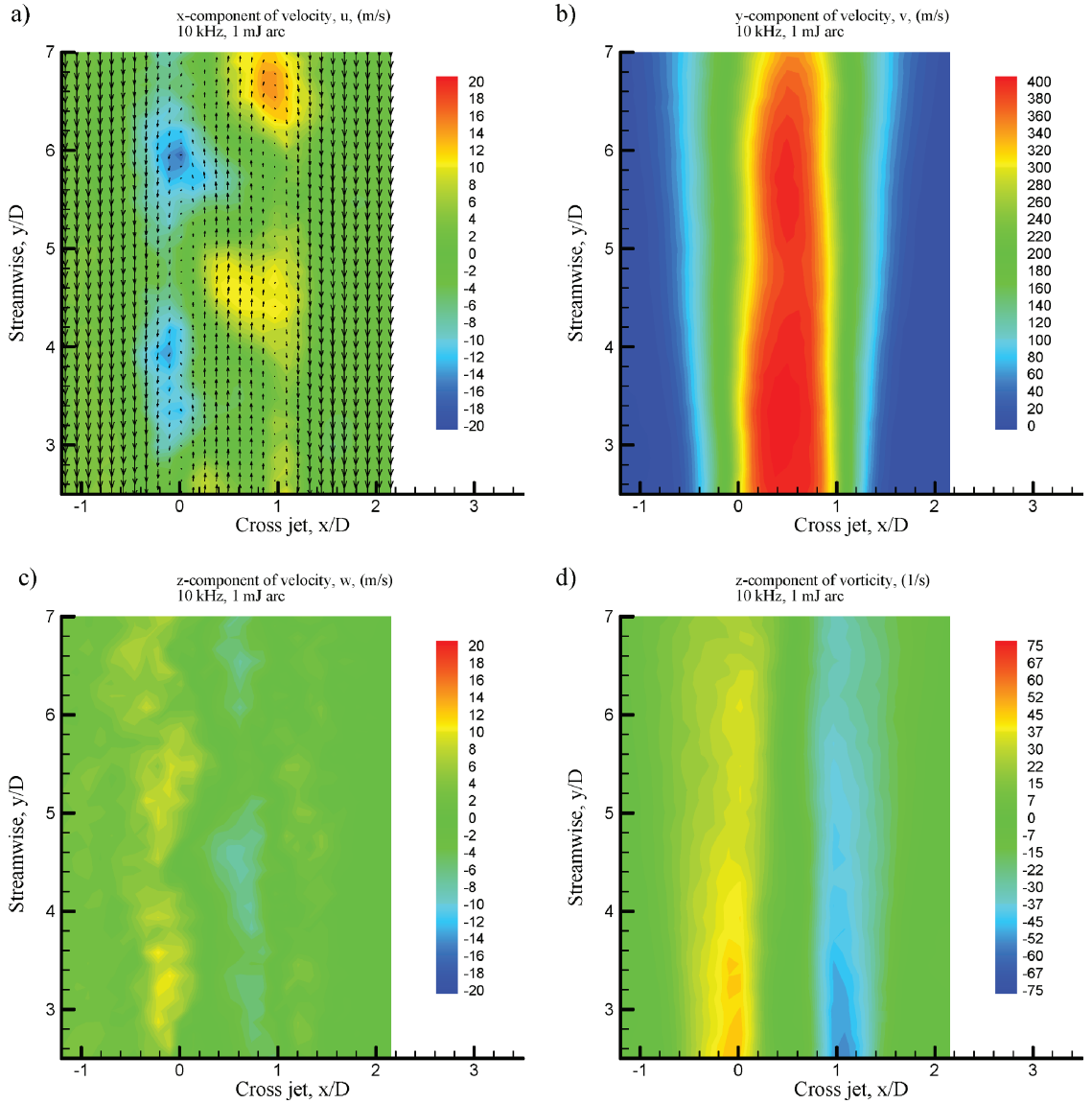

Fig. 15 Contour plots of three Cartesian velocity components [a) u, b) v, c) w, with u–v vector field overlaid on the u component with the convective velocity subtracted] and d) z component of vorticity for Mach 1.38 perturbed by a 10-kHz, 1-mJ arc.

"a larger hammer" is needed to force the shear layer and have an effect on the velocity field (i.e., larger than 1 mJ per disturbance). Of course, this is entirely consistent with data shown in Fig. 8: at 1-mJ/disturbance, the expected shear-shear layer dimension is only slightly above the baseline value.

Conclusions

A method of forcing and controlling supersonic mixing layers has been demonstrated in Mach 1.38, 1.5, and 2.0 axisymmetric jets. Two types of excitation applied to the exit of the jet were investigated: a focused beam from a single-pulsed laser and a multipulse arc. Single laser-pulse excitation induced optical breakdown and was effective in creating a large-scale structure containing well-defined core and braid regions, as determined with the flow visualizations, velocity, and fluctuating static-pressure measurements. The formation of the large-scale structure was apparent over the convective Mach-number range studied from $M_c = 0.63$ to 0.85. The measured convective velocity was found to be higher than the theoretical isentropic values for all Mach numbers (by approximately 25%) and lower than the empirical correction. This structure contained a primary vortex with an elongated secondary structure separated by a stagnation point in a frame of reference moving at the convective velocity. A study of the effect of laser energy on structure formation showed that the large-scale structure formed with as little as 5 mJ of laser energy with the structure size increasing with energy up to 20 mJ above which the effect leveled off. Three-component phase-averaged PIV measurements were obtained to characterize the velocity in the three-dimensional volume around the forced structure. The measurements showed the effect of excitation on the core of the jet (streamwise y velocity isosurface) and on the three-dimensional shape of the structure as defined by the cross-jet x-velocity component. The temporal evolution of the structure was also characterized by PIV measurements showing the growth of the large-scale structure as defined by the vorticity and velocity field indicating a growth rate approximately 2.1 times that in the unperturbed shear layer. Fluctuating static-pressure measurements characterize a large-scale structure with a peak at the braid region (which decreases in magnitude as it convects downstream) and minimum pressure in the primary and secondary vortex cores. Multiple-pulse excitation was investigated using an arc formed at the exit of the jet that was varied in frequency from 5 to 20 kHz. From phase-averaged schlieren images all of the excitation frequencies showed some level of forced structure. The most amplified frequency was qualitatively found to be in the same range as subsonic jets with Strouhal numbers ranging from 0.32 to 0.56. Although the arc provided some perturbation to

the flow, the energy was determined to be to low (∼1 mJ) to have as significant impact on the velocity field compared to the single-pulsed laser excitation case.

Acknowledgment

The authors acknowledge the U.S. Air Force Research Laboratory for their contributions to this research.

References

[1]Leconte, J., "On the Influence of Musical Sounds on the Flame of a Jet of Coal-Gas," *Philosophical Magazine*, 4th Series, Vol. 15, March 1858, pp. 235–239.

[2]Tyndall, J., *Sound*, D. Appleton and Co., New York, 1867, pp. 217–254.

[3]Brown, G. L., and Roshko, A., "On Density Effects and Large Structures in Turbulent Mixing Layers," *Journal of Fluid Mechanics*, Vol. 64, No. 4, 1974, pp. 775–816.

[4]Bogdanoff, D. W., "Compressibility Effects in Turbulent Shear Layers," *AIAA Journal*, Vol. 21, No. 6, 1983, pp. 926, 927.

[5]Papamoschou, D., and Roshko, A., "The Turbulent Compressible Shear Layer: An Experimental Study," *Journal of Fluid Mechanics*, Vol. 197, Dec. 1988, pp. 453–477.

[6]Thurow, B., Samimy, M., and Lempert, W., "Compressibility Effects on Turbulence Structures of Axisymmetric Mixing Layers," *Physics of Fluids*, Vol. 15, No. 6, 2003, pp. 1755–1765.

[7]Fourguette, D. C., Mungal, M. G., and Dibble, R. W., "Time Evolution of the Shear Layer of a Supersonic Axisymmetric Jet," *AIAA Journal*, Vol. 29, No. 7, 1991, pp. 1123–1130.

[8]Murakami, E., and Papamoschou, D., "Eddy Convection in Coaxial Supersonic Jets," *AIAA Journal*, Vol. 38, No. 4, 2000, pp. 628–635.

[9]Gutmark, E. J., Schadow, K. C., and Yu, K. H., "Mixing Enhancement in Supersonic Free Shear Flows," *Annual Review of Fluid Mechanics*, Vol. 27, 1995, pp. 375–417.

[10]Papamoschou, D., "Structure of the Compressible Turbulent Shear Layer," *AIAA Journal*, Vol. 29, No. 5, 1991, pp. 680, 681.

[11]Hall, J. L., Dimotakis, P. E., and Rosemann, H., "Experiments in Nonreacting Compressible Shear Layers," *AIAA Journal*, Vol. 31, No. 12, 1993, pp. 2247–2254.

[12]Clemens, N. T., and Mungal, M. G., "Two- and Three-Dimensional Effects in the Supersonic Mixing Layer," *AIAA Journal*, Vol. 30, No. 4, 1992, pp. 973–981.

[13]Elliott, G. S., Samimy, M., and Arnette, S. A., "The Characteristics and Evolution of Large-Scale Structures in Compressible Mixing Layers," *Physics of Fluids*, Vol. 7, No. 4, 1995, pp. 864–876.

[14]Elliott, G. S., and Samimy, M., "Compressibility Effects in Free Shear Layers," *Physics of Fluids A*, Vol. 2, No. 7, 1990, pp. 1231–1240.

[15]Goebel, S. G., and Dutton, J. C., "Experimental Study of Compressible Turbulent Mixing Layers," *AIAA Journal*, Vol. 29, No. 4, 1991, pp. 538–545.

[16]Murugappan, S., and Gutmark, E., "High Frequency Forcing of an Underexpanded Jet," AIAA Paper 2003-370, Jan. 2003.

[17]Slessor, M. D., Bond, C. L., and Dimotakis, P. E., "Turbulent Shear-Layer Mixing at High Reynolds Numbers: Effects of Inflow Conditions," *Journal of Fluid Mechanics*, Vol. 376, Dec. 1998, pp. 115–138.

[18]Day, M. J., Mansour, N. N., and Reynolds, W. C., "Nonlinear Stability and Structure of Compressible Reacting Mixing Layers," *Journal of Fluid Mechanics*, Vol. 446, Nov. 2001, pp. 375–408.

[19]Urban, W. D., Watanbe, S., and Mungal, M. G., "Velocity Field of the Planar Shear Layer: Compressibility Effects," AIAA Paper 98-0697, Jan. 1998.

[20]Tam, C. K. W., and Zaman, K. B. M. Q., "Subsonic Jet Noise from Nonaxisymmetric and Tabbed Nozzles," *AIAA Journal*, Vol. 38, No. 4, 2000, pp. 592–599.

[21]Papamoschou, D., and Debiasi, M., "Directional Suppression of Noise from a High-Speed Jet," *AIAA Journal*, Vol. 39, No. 3, 2001, pp. 380–387.

[22]Debiasi, M., and Papamoschou, D., "Noise from Imperfectly Expanded Supersonic Coaxial Jets," *AIAA Journal*, Vol. 39, No. 3, 2001, pp. 388–395.

[23]Krothapalli, A., Venkatakrishnan, L., and Lourenco, L., "Crackle: A Dominant Component of Supersonic Jet Mixing Noise," AIAA Paper 2000-2024, June 2000 .

[24]Hileman, J., Thurow, B., and Samimy, M., "Exploring Noise Sources Using Simultaneous Acoustic Measurements and Real-Time Flow Visualizations in Jets," *AIAA Journal*, Vol. 40, No. 12, 2002, pp. 2382–2392.

[25]Callender, B., and Gutmark, E., "A Study of Innovative Techniques in Jet Noise Attenuation," AIAA Paper 2001-0372, Jan. 2001.

[26]Gutmark, E. J., Schadow, K. C., and Yu, K. H., "Mixing Enhancement in Supersonic Free Shear Flows," *Annual Review of Fluid Mechanics*, Vol. 27, 1995, pp. 375–417.

[27]Tillman, T. G., Paterson, R. W., and Presz, W. M., "Supersonic Nozzle Mixer Ejector," *Journal of Propulsion and Power*, Vol. 8, No. 2, 1992, pp.513–519.

[28]Papamoschou, D., "Structure of the Compressible Turbulent Shear Layer," *AIAA Journal*, Vol. 29, No. 5, 1991, pp. 680, 681.

[29]Watanabe, S., and Mungal, M. G., "Velocity Field Measurements of Mixing-Enhanced Compressible Shear Layers," AIAA Paper 99-0088, Jan. 1999.

[30]Zaman, K. B. M. Q., Reeder, M. F., and Samimy, M., "Control of an Axisymmetric Jet Using Vortex Generators," *Physics of Fluids*, Vol. 6, No. 2, 1994, pp. 778–793.

[31]Hileman, J., and Samimy, M., "Effects of Vortex Generating Tabs on Noise Sources in an Ideally Expanded Mach 1.3 Jet," *International Journal of Aeroacoustics*, Vol. 2, No. 1, 2003, pp. 35–63.

[32]Naughton, J. W., and Settles, G. S., "Experiments on the Enhancement of Compressible Mixing Via Streamwise Vorticity: Part I-Optical Measurements," AIAA Paper 92-3549, July 1992.

[33]Yu, K. H., Gutmark, E., Smith, R. A., and Schadow, K. C., "Supersonic Jet Excitation Using Cavity-Actuated Forcing," AIAA Paper 94-0185, Jan. 1994.

[34]Raman, G., and Rice, E. J., "Supersonic Jet Mixing Enhancement Using Impingement Tones from Obstacles of Various Geometries," *AIAA Journal*, Vol. 33, No. 3, 1995, pp. 454–462.

[35]Tam, K. W., and Hu, F. Q., "The Instability of Acoustic Wave Modes of Supersonic Mixing Layers Inside a Rectangular Channel," *Journal of Fluid Mechanics*, Vol. 203, No. June 1989, pp. 51–76.

[36]Doty, M. J., and McLaughlin, D. K., "Experiments on Mach-Wave Interactions in a Compressible Shear Layer," *AIAA Journal*, Vol. 38, No. 10, 2000, pp. 1871–1878.

[37]Murakami, E., and Papamoschou, D., "Experiments on Mixing Enhancement in Dual-Stream Jets," AIAA Paper 2001-0668, Jan. 2001.

[38]Kastner, J., and Samimy, M., "Development and Characterization of Hartmann Tube Fluidic Actuators for High-Speed Flow Control," *AIAA Journal*, Vol. 40, No. 10, 2002, pp. 1926–1934.

[39]Raman, G., Khanafseh, S., Cain, A. B., and Kerschen, E., "Development of High Bandwidth Powered Resonance Tube Actuators with Feedback Control," *Journal of Sound and Vibration*, Vol. 269, No. 3–5, 2004, pp. 1031–1062.

[40]Binder, G., and Didelle, H., "Improvement of Ejector Thrust Augmentation by Pulsating or Flapping Jets," *AGARD Conference of Fluid Dynamics of Jets*, Vol. 308, No. 22, 1981, pp. 1–11.

[41]Lepicovsky, J., Ahuja, K. K., Brown, W. H., and Morris, P. J., "Acoustic Control of Free Jet Mixing," *Journal of Propulsion and Power*, Vol. 2, No. 4, 1986, pp. 323–330.

[42]Kibins, V., and Glezer, A., "Excitation of Supersonic Shear Layers by Piezoelectric Actuators," *Bulletin of the American Physical Society*, Vol. 37, No. 8, 1992, p. 1764.

[43]Cattafesta, L. N., Garg, S., and Shukla, D., "Development of Piezoelectric Actuators for Active Flow Control," *AIAA Journal*, Vol. 39, No. 8, 2001, pp. 1562–1568.

[44]Martens, S., Kinzie, K. W., and McLaughlin, D. K., "Measurements of Kelvin–Helmholtz Instabilities in a Supersonic Shear Layer," *AIAA Journal*, Vol. 32, No. 8, 1994, pp. 1633–1639.

[45]Martens, S., Kinzie, K. W., and McLaughlin, D. K., "Structure of Coherent Instabilities in a Supersonic Shear Layer," *AIAA Journal*, Vol. 34, No. 8, 1996, pp. 1555–1561.

[46]Sandham, N. D., and Reynolds, W. C., "Compressible Mixing Layer: Linear Theory and Direct Simulation," *AIAA Journal*, Vol. 28, No. 4, 1990, pp. 618–624.

[47]Morris, P. J., Grindharan, M. G., and Viswanathan, K., "Turbulent Mixing in Plane and Axisymmetric Shear Layers," AIAA Paper 90-0708, Jan. 1990.

[48]Fourguette, D. C., and Winter, M., "Control of Large-Scale Structure Formation and Vortex Pairing Using Photoacoustic Forcing," *Experiments in Fluids*, Vol. 10, No. 2/3, 1990, pp. 157–160.

[49]Howatson, A. M., *An Introduction to Gas Discharges*, 2nd ed., Pergamon, Elmsford, NY, 1976.

[50]Hoyaux, M. F., *Arc Physics*, Springer-Verlag, New York, 1968.

[51]Raizer, Y. P., *Gas Discharge Physics*, 2nd ed., Springer-Verlag, New York, 1997.

[52]Buck, G. A., and Li, Y., "Numerical and Experimental Studies of Spark-Induced Impulsive Acoustic Disturbances in Compressible Flow," AIAA Paper 2001-0890, Jan. 2001.

[53]Martins, S., Kinzie, K. W., and McLaughlin, D. K., "Wave Structure of Coherent Instabilities in a Planar Shear Layer," AIAA Paper 94-0822, Jan. 1994.

[54]Roth, J. R., Sherman, D. M., and Wilkinson, S. P., "Electrohydrodynamic Flow Control with a Glow-Discharge Surface Plasma," *AIAA Journal*, Vol. 38, No. 7, 2000, pp. 1166–1172.

[55]Roth, J. R., Sherman, D. M., and Wilkinson, S. P., "Boundary Layer Flow Control with a One Atmosphere Uniform Glow Discharge Surface Plasma," AIAA Paper 98-0328, Jan. 1998.

[56]Maker, P. D., Terhune, R. W., and Savage, C. M., "Optical Third Harmonic Generation," *Quantum Electronics, Proceedings of the 3rd International Congress*, edited by P. Grivet and N. Bloembergen, Vol. 2, Columbia Univ. Press, New York, 1964, pp. 1559–1572.

[57]Raizer, Y. P., "Breakdown and Heating of Gases Under the Influence of a Laser Beam," *Soviet Physics USPEKHI*, Vol. 8, No. 5, 1966, pp. 650–673.

[58]Raizer, Y. P., *Laser-Induced Discharge Phenomena*, Consultants Bureau, New York, 1977.

[59]Morgan, G. C., "Laser-Induced Breakdown of Gases," *Reports on Progress in Physics*, Vol. 38, No. 5, 1975, pp. 621–665.

[60]Smith, D. C., "Laser Induced Gas Breakdown and Plasma Interaction," AIAA Paper 2000-0716, Jan. 2000.

[61]Adelgren, R., Elliott, G., Knight, D., Zheltovodov, A., and Beutner, T. J., "Energy Deposition in Supersonic Flows," AIAA Paper 2001-0885, Jan. 2001.

[62]Dors, I., Parigger, C., and Lewis, J., "Fluid Dynamics Effects Following Laser-Induced Optical Breakdown," AIAA Paper 2000-0717, Jan. 2000.

[63]Root, R. G., "Modeling of Post-Breakdown Phenomena," *Laser-Induced Plasmas and Applications*, edited by L. J. Radziemski and D. A. Cremers, Marcel Dekker, New York, 1989, pp. 69–101.

[64]Crawford, J., and Elliott, G. S., "Multiple Laser Excitation for Enhancement of Large-Scale Structures," AIAA Paper 99-0998, Jan. 1999.

[65]Papamoschou, D., "Experimental Investigation of Heterogeneous Compressible Shear Layers," Ph.D. Dissertation, Dept. of Aeronautics, California Inst. of Technology, Pasadena, CA, 1986.

[66]Ho, C. M., and Huerre, P., "Perturbed Free Shear Layers," *Annual Review of Fluid Mechanics*, Vol. 16, 1984, pp. 365–424.

[67]Adelgren, R. G., Elliott, G. S., Crawford, J. B., Carter, C. D., Grosjean, D., and Donbar, J. M., "Axisymmetric Jet Shear Layer Excitation Induced by Electric Arc Discharge and Focused Laser Energy Deposition," AIAA Paper 2002-0729, Jan. 2002.

M. Auweter-Kurtz
Associate Editor